View Article Online / Journal Homepage / Table of Contents for this issue

Growth of epitaxial zirconium-doped indium oxide (222) at low temperature by rf sputtering

Yuan-Chang Liang*[a] and Hsin-Yi Lee*[bc]

Received 22nd March 2010, Accepted 25th May 2010
DOI: 10.1039/c004452k

Published on 17 June 2010. Downloaded by National Chiao Tung University on 25/04/2014 06:48:18.

Zr-doped In_2O_3 (Zr-In_2O_3) (222) epitaxial layers of thickness 210 nm were grown on yttria-stabilized zirconia (YSZ) (111) and Al_2O_3 (0001) substrates with rf magnetron sputtering at 350 °C in an atmosphere deficient in oxygen. X-Ray scattering and use of a transmission electron microscope (TEM) revealed Zr-In_2O_3 films to be deposited epitaxially on YSZ (111) and Al_2O_3 (0001). Images observed with an atomic-force microscope demonstrate that the substrate profoundly affected the topography of the Zr-In_2O_3 (222) epilayers. The large mismatch of the Zr-In_2O_3 (222)/Al_2O_3 (0001) heteroepitaxy was responsible for the surface structure of the epilayer being rougher than that on YSZ (111). Cross-sectional TEM images reveal dense crystalline films with no macroscopic imperfection; the crystalline order of Zr-In_2O_3 epilayers is preserved up to the top surface. The Zr-In_2O_3 (222)/YSZ (111) heteroepitaxy has a Hall mobility greater than that of Zr-In_2O_3 (222)/Al_2O_3 (0001), perhaps due to the greater lattice mismatch of the Zr-In_2O_3 (222)/Al_2O_3 (0001) heteroepitaxy that results in Zr-In_2O_3 having a poor crystalline quality. Domain boundaries on a nanometre scale were found in the heteroepitaxial Zr-In_2O_3 (222)/Al_2O_3 (0001) resulting from random nucleation and relaxation of misfit stress. The existence of these domain boundaries on a nanometre scale thus affects the electrical properties of the Zr-In_2O_3 epilayer.

1. Introduction

Transparent conductive oxides (TCOs) attract attention because they are widely used in heat-reflecting mirrors, as transparent conducting electrodes for optoelectronic devices, and as window electrodes for solar cells.[1–3] Indium oxide (In_2O_3) is the most common, optically transparent, electronic conductor, and its optoelectronic properties improve on doping with cations of higher valence.[4] Most research on the structural characteristics of impurity-doped In_2O_3 films has focused on the effects of processing conditions.[5] Many authors have investigated polycrystalline or amorphous film structures grown at a low temperature on glass or plastic substrates,[6] but understanding the surface morphology of materials in this class depends on characterizing the growth of a film on a single-crystalline substrate. There have been only few investigations of the physical properties of heteroepitaxial Sn-doped In_2O_3 films or In_2O_3 films on yttria-stabilized zirconia (YSZ) substrates with (400) or (222) crystallographic orientations.[7,8] No conclusive evidence of the effects of the substrate on the surface morphology for a particular crystallographic orientation under identical processing conditions, and on the properties of In_2O_3 films, is available. Furthermore, these In_2O_3 epilayers were fabricated at a temperature greater than 650 °C.[7,8] For deposition of a thin film, as the growth temperature is increased, the grain size and, therefore, the surface roughness of the thin films increase.[9] A decreased temperature for the growth of oxide heteroepitaxy might also decrease the extent of interdiffusion at the interface.[10] Bourlange *et al.* reported that In_2O_3 films grown on YSZ substrates at temperatures 650–900 °C have a distinct island structure together with a large root-mean-square roughness, about 10–100 nm.[8] This rough structure of a thin film resulting from its growth at a high temperature might decrease the reliability of nanodevices when such TCO films serve as a contact electrode. For these reasons, transparent, conductive indium oxide is fabricated preferably at a temperature less than 600 °C for practical applications.

To achieve an understanding of the basic physical properties of this material, an investigation of such films grown at a lower temperature and with epitaxy is thus desirable. In particular, the local structure and electrical properties of such films on a nanometre scale are not understood, which might reflect the complicated structure of indium oxide. Conductive atomic-force microscopy enables the electrical properties to be correlated with the surface topography on a nanometre scale; this technique has been applied to III–V semiconductor heterostructures.[11,12] Here, we report the crystallographic characteristics and nanostructural conductive properties of zirconium-doped films of indium oxide having (222) epitaxy on two single-crystalline substrates grown with rf magnetron sputtering. We investigated the structure and electrical properties on a nanometre scale of the surface of Zr-doped In_2O_3 (222) epitaxy on YSZ (111) and Al_2O_3 (0001).

2. Experimental

Zr-doped In_2O_3 (Zr-In_2O_3) films were grown on single-crystalline YSZ (111) and Al_2O_3 (0001) substrates using rf magnetron sputtering. In_2O_3 crystallizes on the adopted target in the cubic bixbyite structure with a lattice parameter 1.011 nm. The yttria

[a]*Institute of Materials Engineering, National Taiwan Ocean University, Keelung, 20224, Taiwan. E-mail: hylee@nsrrc.org.tw; deanvera@yahoo.com.tw*
[b]*National Synchrotron Radiation Research Center, 101 Hsin-Ann Road, Hsinchu Science Park, 30076, Taiwan*
[c]*Department of Materials Science and Engineering, National Chiao Tung University, Hsinchu, 300, Taiwan*

 This journal is © The Royal Society of Chemistry 2010

View Article Online

Published on 17 June 2010. Downloaded by National Chiao Tung University on 25/04/2014 06:48:18.

content in YSZ substrates is 15% and the YSZ substrate has a cubic structure with lattice parameter 0.513 nm. The bulk lattice parameters of the Al_2O_3 substrate are $a = 0.475$ nm and $c = 1.299$ nm. The target adopted in the experiment was prepared on mixing the precursor oxide powders of ZrO_2 (5 mass%) and In_2O_3 (95 mass%), pressing the powders into a pellet, and sintering that to a large density. The chosen composition of the initial target was based on literature information that Zr-doped In_2O_3 films with a Zr/In ratio 0.057–0.065 have satisfactory conductivity.[13] The composition of the film as deposited was evaluated with X-ray photoelectron spectra (XPS) in the Zr 3d, In 3d and O 1s regions. The Zr-In_2O_3 films were grown on YSZ (111) and Al_2O_3 (0001) substrates in the same run, with the substrates placed in the central part of the heater holder. Multiple samples with the same heteroepitaxial system were made to check the reproducibility of this study. The thickness of the Zr-In_2O_3 film was fixed at about 210 nm; the distance between the target and substrate was 75 mm. The vacuum chamber was evacuated to a base pressure of about 8×10^{-7} Torr before deposition. The growth temperature of the Zr-In_2O_3 films was maintained at 350 °C. The pressure of pure gaseous Ar during deposition of Zr-In_2O_3 films was fixed at 5 mTorr.

The crystallographic structures of the Zr-In_2O_3 films were analyzed with measurements of high-resolution X-ray diffraction (XRD) with Cu Kα radiation from a synchrotron X-ray source at wiggler beamline BL17B1 in the National Synchrotron Radiation Research Center (NSRRC), Hsinchu, Taiwan. The surface morphology of the Zr-In_2O_3 films was investigated with an atomic-force microscope (AFM). The surface–current images of Zr-In_2O_3 films were observed using a conductive atomic-force microscope (CAFM) with PtIr tips; these observations were conducted on an area 1 × 1 μm². Thin slices for analysis with a high-resolution, transmission electron microscope (HRTEM) were prepared with a dual-beam focused-ion-beam instrument. The areas selected for cutting with an ion beam were protected with an amorphous carbon overlayer. HRTEM observations were performed with an electron microscope (JEOL 2100F, 200 kV).

The carrier concentration and mobility were determined with a Hall-measurement system (Ecopia HMS-3000) with the van der Pauw technique near 295 K.

3. Results and discussion

To determine the effect of the processing conditions on the composition of the Zr-In_2O_3 film as deposited, we measured X-ray photoelectron spectra. Fig. 1 presents wide-scan XPS of a Zr-In_2O_3 film grown on a sapphire substrate. The inset in Fig. 1 shows a comparison of the experimental and simulated O 1s spectra. The O 1s component at ~530.3 eV is attributed to oxygen in the oxide crystal and the O 1s component at 531.2 eV represents oxygen ions in oxygen-deficient regions. According to a calculation from narrow scans of the XPS in the Zr 3d, In 3d5 and O 1s regions, the film has a composition $In_{1.89}Zr_{0.11}O_{2.37}$. The oxygen content in the film deviates slightly from stoichiometric proportions, perhaps because the film was deposited in an atmosphere in which oxygen was deficient.[14]

Fig. 2 shows XRD patterns of Zr-In_2O_3 films (thickness 210 nm) grown on various single-crystalline substrates, with

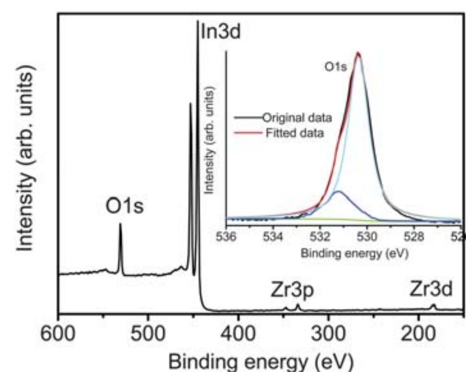

Fig. 1 XPS of a Zr-In_2O_3 film deposited on a sapphire substrate. The inset shows the experimental and simulated results of the O 1s spectrum. Oxygen was deficient in the film.

(222) Bragg reflections on YSZ (111) and Al_2O_3 (0001) substrates. The absence of a ZrO_2 phase from XRD patterns with a wide angular range (not shown here) indicates the effective solid solution of Zr in the In_2O_3 films. Out-of-plane rocking curves of the Zr-In_2O_3 films are shown in the insets. The values for the full width at half maximum (FWHM) of the rocking curves at the Zr-In_2O_3 (222) Bragg reflection are 0.42° for films grown on YSZ (111) and 0.58° for Al_2O_3 (0001) substrates; the

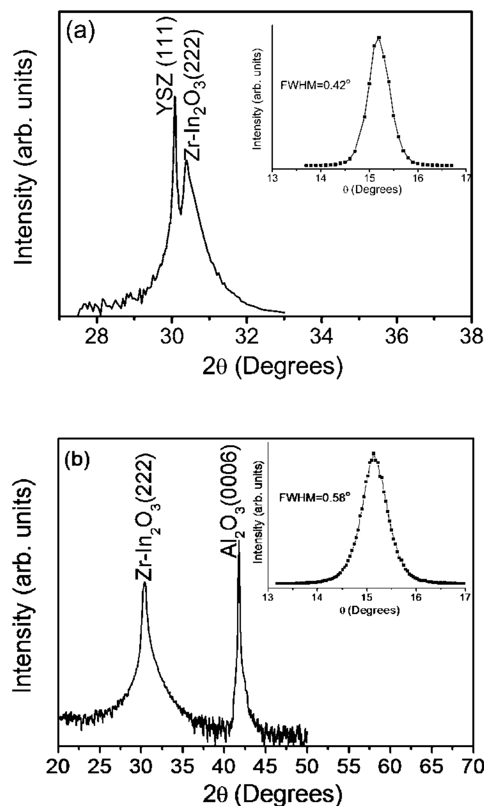

Fig. 2 High-resolution XRD θ–2θ profiles for (a) Zr-In_2O_3/YSZ and (b) Zr-In_2O_3/Al_2O_3. The corresponding rocking curves of (222) Bragg reflections of Zr-In_2O_3 are shown in the insets. The values for the full width at half maximum of the rocking curves at the Zr-In_2O_3 (222) growth on YSZ and Al_2O_3 are 0.42° and 0.58°, respectively.

View Article Online

Published on 17 June 2010. Downloaded by National Chiao Tung University on 25/04/2014 06:48:18.

FWHM values are 0.027° for the YSZ substrate (111) (0001) and 0.021° for Al_2O_3 (111) (0001). The lattice distortion ($\Delta d/d_{hkl}$) is defined as $(d_{exp} - d_{hkl})/d_{hkl}$; d_{exp} denotes the distance between the indicated planes, derived from the experimental peak position by means of the Bragg formula, and d_{hkl} is the theoretical value calculated from the lattice parameter (1.011 nm).[15] The lattice distortion was compared with the (222) Bragg reflections. The lattice distortion of the Zr-In_2O_3 film on YSZ (111) was 0.41%, and that of a film grown on an Al_2O_3 (0001) substrate was slightly larger, 0.55%. As the ionic radius of In^{3+} is 80 pm and that of Zr^{4+} is 72 pm, a partial substitution of In^{3+} by Zr^{4+} might cause a slightly decreased axis length; the lattice distortion of the Zr-In_2O_3 films as deposited on YSZ (111) and Al_2O_3 (0001) substrates might originate from crystalline defects in the films.

ϕ-Scans of the Zr-In_2O_3 (004) Bragg reflections show clear three-fold rotational symmetry on the YSZ (111) substrate and six-fold rotational symmetry on the Al_2O_3 (0001) substrate, revealing satisfactory in-plane crystalline orientation of the Zr-In_2O_3 films on these single-crystalline substrates (Fig. 3(a) and (b)). The FWHM of Zr-In_2O_3 (004) on YSZ (111) is 0.42°, but a large value 1.73° was found for a film grown on the Al_2O_3 (0001) substrate, which might reflect a decreased crystalline quality in the plane for the Zr-In_2O_3/Al_2O_3 heteroepitaxy.

The TEM images of Zr-In_2O_3/YSZ and Zr-In_2O_3/Al_2O_3 were recorded with an incident electron beam parallel to direction $[1\bar{1}\bar{2}]$ of the YSZ substrate and direction $[10\bar{1}0]$ of the Al_2O_3 substrate. Low-resolution cross-sectional TEM images (Fig. 4(a) and (b)) of Zr-In_2O_3 layers on YSZ and Al_2O_3 substrates reveal dense crystalline films with no macroscopic imperfection; the thickness of the Zr-In_2O_3 layers was about 210 nm, conforming to the design value. Fig. 4(c) and (d) present HRTEM images of the Zr-In_2O_3/YSZ and Zr-In_2O_3/Al_2O_3 interfaces showing the epitaxial growth of Zr-In_2O_3 on the YSZ and Al_2O_3 substrates. The interface of the heteroepitaxial systems of Zr-In_2O_3/YSZ and Zr-In_2O_3/Al_2O_3 is atomically sharp; neither intermediate phase nor chemical reaction is observed at the interface. Lattice fringes of three kinds are readily distinguished in the HRTEM image; Fig. 5 shows that the crystalline order is preserved up to the top surface of Zr-In_2O_3/Al_2O_3, a characteristic not observed for Zr-In_2O_3/YSZ. The insets show the corresponding fast-Fourier-transform (FFT) patterns of local lattice fringes in each domain. According to the results of XRD, Zr-In_2O_3/Al_2O_3 has an epitaxial structure with a perfect orientation (222). That the FWHM value of Zr-In_2O_3/Al_2O_3 is larger than that of Zr-In_2O_3/YSZ indicates that crystalline defects might be favored to exist in Zr-In_2O_3/Al_2O_3. The variously oriented domains in Zr-In_2O_3 on Al_2O_3 are attributed to the large mismatch (−13.2%) between lattices of In_2O_3 (222) and Al_2O_3 (0001).[16] The formation of various orientations in the crystal explains the observed domains, as reported for perovskite and other oxide thin films grown on substrates with lattice mismatch.[17,18] That formation is attributed to the relaxation of

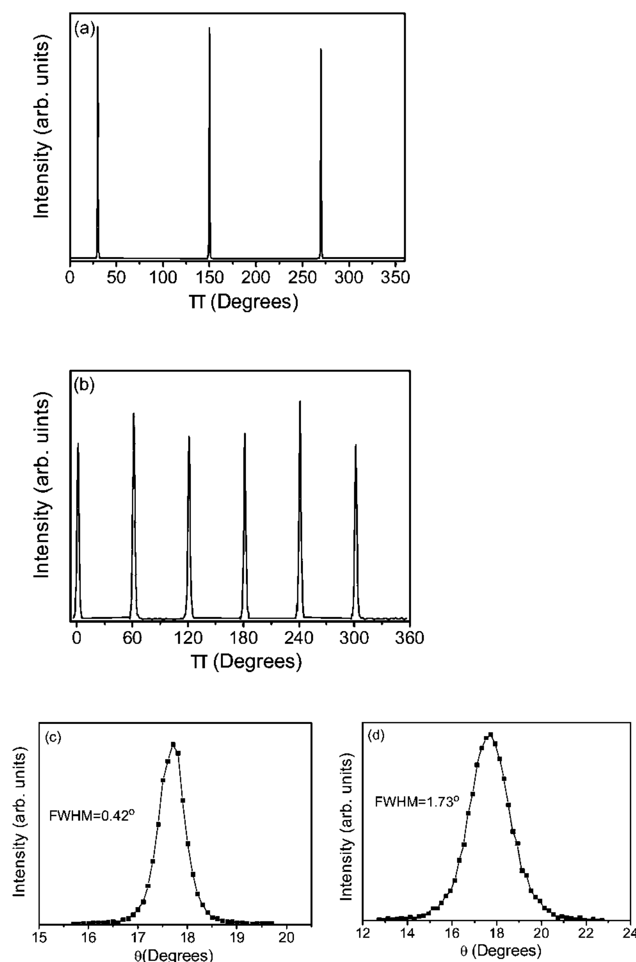

Fig. 3 (004) ϕ-Scan profiles for (a) Zr-In_2O_3/YSZ and (b) Zr-In_2O_3/Al_2O_3. The corresponding rocking curves of (004) Bragg reflections of Zr-In_2O_3 on YSZ and Al_2O_3 are shown in (c) and (d), respectively. The ϕ-scan profiles reveal satisfactory in-plane crystalline orientation of Zr-In_2O_3 films on these single-crystalline substrates.

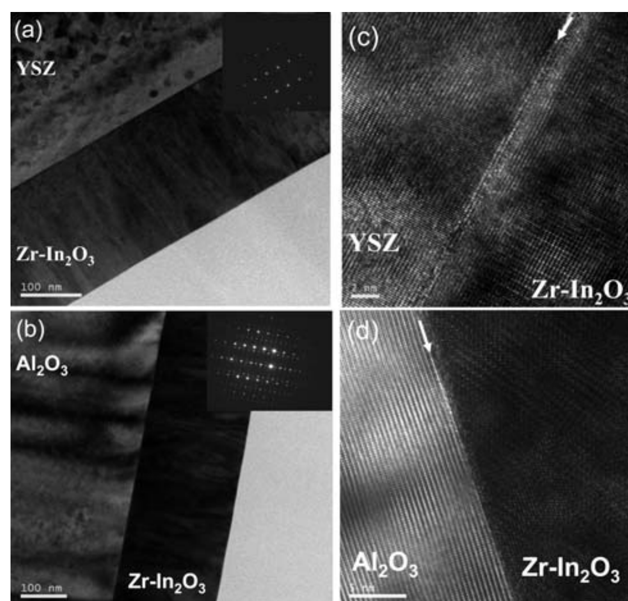

Fig. 4 Cross-sectional TEM images at small magnification of (a) Zr-In_2O_3/YSZ and (b) Zr-In_2O_3/Al_2O_3. The images show that the Zr-In_2O_3 epilayers have a smooth film for the surface structure. The corresponding electron-diffraction patterns as shown in the insets were recorded in an area of the heterointerface. HRTEM images show epitaxial growth of Zr-In_2O_3 films on (c) YSZ and (d) Al_2O_3 substrates. Interfaces are marked with white arrows.

 This journal is © The Royal Society of Chemistry 2010

View Article Online

Published on 17 June 2010. Downloaded by National Chiao Tung University on 25/04/2014 06:48:18.

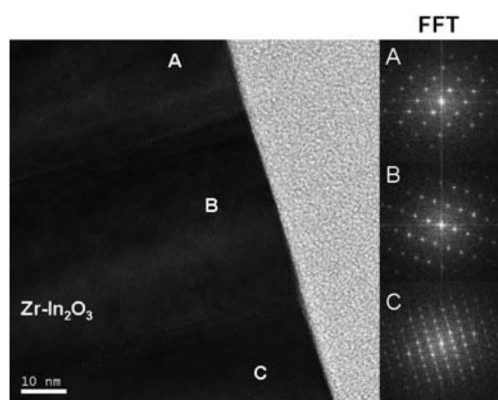

Fig. 5 This HRTEM image shows multi-domain boundaries in Zr-In_2O_3 film on an Al_2O_3 substrate. The corresponding FFT of each domain is also exhibited.

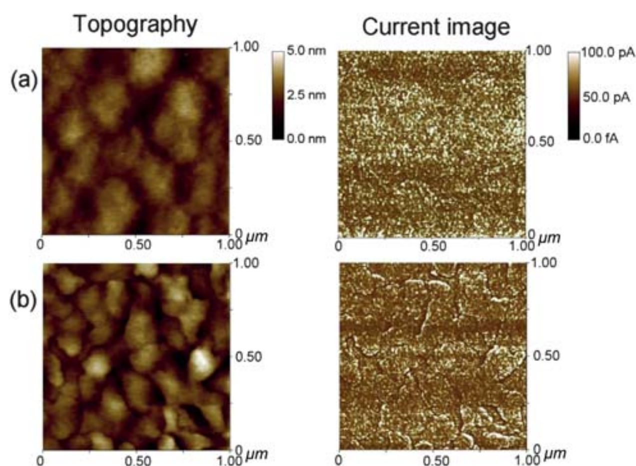

Fig. 6 Surface topography and the corresponding current images of Zr-In_2O_3 films grown on (a) YSZ and (b) Al_2O_3 substrates. The current image of the Zr-In_2O_3 epilayer on an Al_2O_3 substrate clearly reveals an enhanced current conduction at the edges of the islands.

misfit stress between the film and the substrate; experiments have confirmed that a mixture of oriented domains occurs with increasing film thickness, and these boundaries on a nanometre scale combine the discrete oriented domains to form a continuous film as exhibited in the HRTEM image.

The surface morphology of the epitaxial Zr-In_2O_3 films was measured with an atomic-force microscope. All Zr-In_2O_3 epilayers reveal smooth surfaces with neither crack nor pinhole. Fig. 6 shows a three-dimensional (3D) structure of Zr-In_2O_3 epilayers on YSZ (111) and Al_2O_3 (0001) substrates. The film surface comprises a grain structure more rounded on the YSZ substrate than on the Al_2O_3 substrate. Spirally shaped surface grains and triangularly shaped crystallites of heteroepitaxial In_2O_3 (222)/YSZ (111) are reported for thin films from pulsed-laser deposition and e-beam evaporation.[7,19] The method of thin-film preparation clearly affects profoundly the growth mechanism of the epilayer of In_2O_3 on YSZ (111) substrates. The Zr-In_2O_3 epilayer on YSZ exhibits an average surface grain size of ~400 nm, and that on Al_2O_3 is ~220 nm. The difference in the growth mode indicates that the rate of migration of atoms deposited on YSZ (111) is greater than that on Al_2O_3 (0001). The Zr-In_2O_3 epilayer on YSZ has a root-mean-square (rms) surface roughness of 0.42 nm, compared with 0.58 nm for the surface of the Zr-In_2O_3 epilayer on an Al_2O_3 substrate (Fig. 6(b)). The matching of the crystalline structures and lattice parameters between YSZ and Zr-In_2O_3 is superior to that for the Zr-In_2O_3/Al_2O_3 heteroepitaxy. As all films were grown under the same processing conditions, a smaller lattice mismatch between the film and the substrate might decrease the rms surface roughness of Zr-In_2O_3 on the YSZ substrate.[20–22] The current images that correspond to AFM images measured at a small applied bias, 0.15 V, during AFM scanning, which reflect the local nano-structural conductivity of the films, are displayed also in Fig. 6. According to these current–voltage (*I–V*) measurements, the white regions appearing in the measured area have a nonlinear *I–V* characteristic; electron tunneling of Fowler–Nordheim type is responsible for the detected currents over the measured regions.[23] The Zr-In_2O_3 epilayer on the YSZ substrate has white regions over the area of interest under the applied bias. The current image shows a current map that is well balanced. A comparison between the current image and the topography revealed no obvious relation between the topography and the local conductivity. The surface of the Zr-In_2O_3 epilayer on an Al_2O_3 substrate exhibits a 3D, island-like feature, and the corresponding current image in Fig. 6(b) clearly reveals an enhanced current conduction at the edges of the islands. The greatest currents are detected along the edges of prominent features, indicating that the crystallographic features at such locations are more electrically active than other parts in the matrix. An effect of topography on the detected currents is here excluded as the thickness variation due to the surface grain structure is ~8 nm, which is less than 4% of the total thickness of the film. The hexagonal-island surface feature of a GaN film as grown is also associated with increased conduction in the island sidewalls.[12,24] The surface-crystallographic defects affect the surface conductivity under a small applied voltage. Carriers supplied by oxygen vacancies or In interstitial atoms on the epi-layer surface contribute to the electrical properties of the surface. The carrier densities of Zr-In_2O_3 epilayers measured from the Hall effect are 1.33×10^{21} cm^{-3} on YSZ substrates and 1.42×10^{21} cm^{-3} on Al_2O_3 substrates. No marked difference in the magnitude of carrier density exists between these samples, which might be due to these epilayers being fabricated in the same run, but the mobility of Zr-In_2O_3/YSZ, 32.7 cm^2 V^{-1} s^{-1}, is larger than that of Zr-In_2O_3/Al_2O_3, 24.4 cm^2 V^{-1} s^{-1}. The mobility of In_2O_3 films is reported to be strongly correlated with the randomness of crystallographic structures in the film.[25] The superior mobility of the Zr-In_2O_3 epilayer on YSZ is revealed by the fact that the crystallographic planes of the Zr-In_2O_3 epilayer are more compact than those grown on Al_2O_3. This condition is verified from both XRD and HRTEM results shown earlier, but it is difficult to evaluate the chemistry of minute surface defects in this work with a high-resolution scanning probe microscope under ultra-high vacuum. According to our experimental results, the existence of domain boundaries extending to the film surface in the Zr-In_2O_3/Al_2O_3 heteroepitaxy might contribute to the poor surface structure. Moreover, these nanometre-scale boundaries might modify the electronic energies of the surface of the Zr-In_2O_3 epilayer on Al_2O_3, which would further result in larger

View Article Online

Published on 17 June 2010. Downloaded by National Chiao Tung University on 25/04/2014 06:48:18.

detected currents along the edges of some prominent features during the CAFM measurement.

4. Conclusion

For Zr-In_2O_3 (222) epilayers of thickness 210 nm grown on YSZ (111) and Al_2O_3 (0001) substrates with rf magnetron sputtering, we observed a smooth surface with a 3D, island-like feature of Zr-In_2O_3 (222) epilayers on the single-crystalline substrates. The large lattice mismatch between Zr-In_2O_3 (222) and Al_2O_3 (0001) is responsible for the surface structure of the epilayer being rougher than that on YSZ. The FWHM values of out-of-plane and in-plane rocking curves indicate the crystalline quality of the Zr-In_2O_3 epilayer on YSZ to be superior to that on an Al_2O_3 substrate. TEM observations reveal that the crystalline order of Zr-In_2O_3 epilayers is preserved up to the top surface, and domain boundaries on a nanometre scale were found in the Zr-In_2O_3 (222)/Al_2O_3 (0001) heteroepitaxy with the HRTEM because of random nucleation and the relaxation of misfit stress. The existence of domain boundaries on a nanometre scale might modify the electronic energy levels of the surface of a Zr-In_2O_3 epilayer on Al_2O_3, which would result in increased detected currents along the edges of prominent features during the CAFM measurement. Defects of this kind might also decrease the Hall mobility of a Zr-In_2O_3 epilayer on an Al_2O_3 substrate.

Acknowledgements

We acknowledge the financial support from the National Science Council of the Republic of China (Grant No. NSC 97-2221-E-270-004 and NSC 97-2221-E-213-001) and the National Taiwan Ocean University (Grant No. NTOU-RD-AA-2010-104031).

References

1 P. Nath and R. F. Bunshah, *Thin Solid Films*, 1980, **69**, 63.
2 V. Korobov, M. Leibovitch and Y. Shapira, *J. Appl. Phys.*, 1993, **74**, 3251.
3 M. Higuchi, S. Uekusa, R. Nakano and K. Yokogawa, *J. Appl. Phys.*, 1993, **74**, 6710.
4 T. Koida and M. Kondo, *J. Appl. Phys.*, 2007, **101**, 063713.
5 A. V. Mudryi, A. V. Ivaniukovich and A. G. Ulyashin, *Thin Solid Films*, 2007, **515**, 6489.
6 J. Lee, H. Jung, J. Lee, D. Lim, K. Yang, J. Yi and W. C. Song, *Thin Solid Films*, 2008, **516**, 1634.
7 H. Ohta, M. Orita, M. Hirano and H. Hosono, *J. Appl. Phys.*, 2002, **91**, 3547.
8 A. Bourlange, D. J. Payne, R. G. Palgrave, J. S. Foord, R. G. Egdell, R. M. J. Jacobs, A. Schertel, J. L. Hutchison and P. J. Dobson, *Thin Solid Films*, 2009, **517**, 4286.
9 Y. C. Liang, Y. C. Liang and J. P. Chu, *Electrochem. Solid-State Lett.*, 2008, **11**, G41.
10 H. Y. Lee, H. J. Liu, Y. C. Liang, K. F. Wu and C. H. Lee, *J. Electrochem. Soc.*, 2009, **156**, G114.
11 X. A. Cao, J. M. Teetsov, M. P. D'Evelyn, D. W. Merfeld and C. H. Yan, *Appl. Phys. Lett.*, 2004, **85**, 7.
12 J. W. P. Hsu, M. J. Manfra, D. V. Lang, S. Richter, S. N. G. Chu, A. M. Sergent, R. N. Kleiman, L. N. Pfeiffer and R. J. Molnar, *Appl. Phys. Lett.*, 2001, **78**, 1685.
13 H. Kim, J. S. Horwitz, G. P. Kushto, S. B. Qadri, Z. H. Kafafi and D. B. Chrisey, *Appl. Phys. Lett.*, 2001, **78**, 1050.
14 S. Boycheva, A. K. Sytchkova, M. L. Grilli and A. Piegari, *Thin Solid Films*, 2007, **515**, 8469.
15 W. F. Wu, B. S. Chiou and S. T. Hsieh, *Semicond. Sci. Technol.*, 1994, **9**, 1242.
16 Z. X. Mei, Y. Wang, X. L. Du, Z. Q. Zeng, M. J. Ying, H. Zheng, J. F. Jia, Q. K. Xue and Z. Zhang, *J. Cryst. Growth*, 2006, **289**, 686.
17 R. A. Rao, D. Lavric, T. K. Nath, C. B. Eom, L. Wu and F. Tsui, *Appl. Phys. Lett.*, 1998, **73**, 3294.
18 C. H. Hsu, P. Chang, W. C. Lee, Z. K. Yang, Y. J. Lee, M. Hong, J. Kwo, C. M. Huang and H. Y. Lee, *Appl. Phys. Lett.*, 2006, **89**, 122907.
19 N. Taga, H. Odaka, Y. Shigesato, I. Yasui, M. Kamei and T. E. Haynes, *J. Appl. Phys.*, 1996, **80**, 978.
20 Y. C. Liang, H. Y. Lee, H. J. Liu, C. K. Huang and T. B. Wu, *J. Cryst. Growth*, 2005, **279**, 114.
21 Y. C. Ling and Y. C. Liang, *J. Electrochem. Soc.*, 2007, **154**, G193.
22 Y. C. Liang and Y. C. Liang, *J. Cryst. Growth*, 2007, **304**, 275.
23 S. K. So, W. K. Choi, C. H. Cheng, L. M. Leung and C. F. Kwong, *Appl. Phys. A: Mater. Sci. Process.*, 1999, **68**, 447.
24 E. J. Miller, D. M. Schaadt, E. T. Yu, C. Poblenz, C. Elsass and J. S. Speck, *J. Appl. Phys.*, 2002, **91**, 9821.
25 K. Ellmer, *J. Phys. D: Appl. Phys.*, 2000, **33**, R17.

 This journal is © The Royal Society of Chemistry 2010